

<https://doi.org/10.1038/s43247-024-01627-w>

# Global mantle isotopic anomalies linked to supercontinent-super ocean evolution for the past 700 million years

**Piero A. B. de Sampaio** <sup>1,2</sup>, **Zheng-Xiang Li** <sup>1,2</sup> & **Luc S. Doucet** <sup>1,2,3</sup>

Earth's mantle isotopic composition is highly heterogeneous, with enriched and depleted regions<sup>1-3</sup> shaped by a complex history of depletion and re-enrichment over 4.5 billion years. The spatial configuration of large-scale heterogeneity in the mantle is not random<sup>4,5</sup>, but the timing and mechanisms that caused such heterogeneity are still debated<sup>2,6,7</sup>. We compiled radiogenic isotope data of mid-ocean ridge and plume-induced basalts from both present-day and past oceans for the past 900 million years of the relatively isotopically enriched African mantle domain. Our analysis shows that oceanic rocks of the African mantle domain exhibit a relatively homogenous composition similar to the prevalent mantle estimates (PREMA<sup>8</sup>) until ca. 350 million years ago when plume-derived rocks started becoming isotopically enriched with maximum enrichment reached in the mid-Cretaceous. From that point in time, plume-derived rocks shift toward depletion, getting closer to the prevalent mantle value. The enrichment trend is interpreted to have resulted from the recycling of crustal material during the assembly and the early stage of a break-up of Gondwana and Pangea, whereas the subsequent depletion trend is due to the outward retreat of the subduction girdle during the break-up of Pangea, thus both are legacies of geodynamic processes related to the supercontinent cycle.

The Earth's mantle as sampled by its melting products is remarkably heterogeneous. Both mantle-derived basaltic rocks formed along mid-ocean ridges, and plume-induced igneous rocks, display a wide range of distinct isotopic compositions that reflect the long history of mantle depletion and recycling processes<sup>1-3</sup>. Mixing of melts from compositional endmembers or mantle source regions can explain most observed isotopic variabilities in such rocks. One particular end member, the enriched mantle (EM), is believed to be caused by the recycling of continental crustal or lithospheric material<sup>2,3,9,10</sup>. It has long been recognised that the geographic distribution of rocks with EM signatures is not random, with a North-South isotopic dichotomy being first suggested based on the prevalence of EM compositions in the southern hemisphere<sup>6,7</sup>, with two enrichment maxima located in the Indian and South-Atlantic Oceans (the Dupal anomaly)<sup>4</sup> and the South Pacific Ocean (SOPITA)<sup>11</sup>, respectively. Such enrichment features were often regarded to have been a long-lived feature of the mantle, perhaps even a primordial feature<sup>5</sup>. More recently, an east-west hemispheric isotopic dichotomy was identified using samples from deep plumes in the present-day ocean, with a more depleted Pacific mantle domain and a more enriched African mantle domain (Fig. 1a) divided by the circum-Pacific subduction

girdle, interpreted to reflect distinct evolutionary histories of the two domains during the Rodinia and Pangea supercontinent cycles<sup>12</sup>. According to this latter model, the African mantle domain received preferential enrichment during the multiple subduction-collision events responsible for the formation of Gondwana and eventually the supercontinent Pangea, along with ongoing subductions during the existence and later breakup of the supercontinent; whereas the Pacific mantle domain largely avoided of such enrichment since its inception during the breakup of the previous supercontinent Rodinia<sup>12,13</sup>.

One way to better understand the formation mechanism of such large-scale mantle heterogeneity, and thus potentially to verify the two contrasting mantle dichotomy models, is to examine the starting age of such enrichment. So far, our understanding of the present-day mantle isotopic composition relied entirely on mantle-derived basaltic rocks from the present-day oceanic lithosphere, which is limited to the last 200 Ma<sup>14</sup> due to recycling of oceanic lithosphere at convergent margins. However, fragments of older oceanic lithosphere are found as parts of subduction-accretion complexes and obducted ophiolitic complexes in old orogens<sup>15</sup>. Such rocks would allow us to peer into the isotopic composition of the mantle underlying the now-closed

<sup>1</sup>Earth Dynamics Research Group (EDRG), The Institute for Geoscience Research (TIGeR), School of Earth and Planetary Sciences, Curtin University, Perth, WA, Australia. <sup>2</sup>Earth Evolution and Dynamics Research Center (EDRC), Laoshan Laboratory, Qingdao, 266237, China. <sup>3</sup>State Key Laboratory of Geological Processes and Mineral Resources, China University of Geosciences, Wuhan, Hubei, 430074, China. e-mail: piero\_sampaio@postgrad.curtin.edu.au; z.li@curtin.edu.au

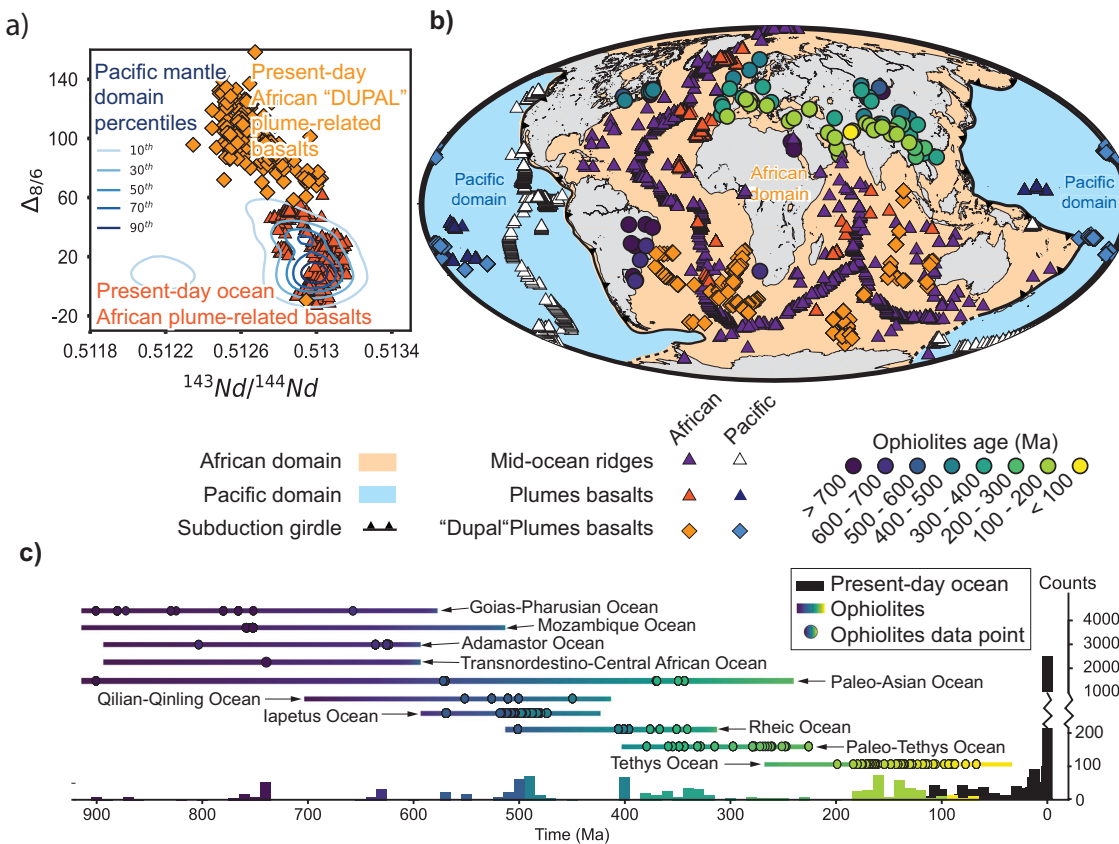


**Fig. 1 | Spatiotemporal distribution of ophiolites.** **a**  $^{143}\text{Nd}/^{144}\text{Nd}$  vs.  $\Delta_{8/6}$ <sup>5</sup> scatter plot from deep mantle plume-derived basalts from reference<sup>12</sup>. Kernel density contours for Pacific Mantle Domain basalts are overlaid on top of scatter points of African mantle domain samples. **b** Present-day spatial distribution of ophiolites of the African mantle domain from which samples were used and colour-coded for age; also shown are sample locations of normal-oceanic crust basalts and plume-derived

basalts from the African and Pacific domains. See methods for data sources. **c** Temporal distribution of ophiolites of the African mantle domain, all assigned to respective past oceanic basins from which the ophiolites were derived (see Supplementary Fig. 1). The bar chart at the bottom shows the number of Nd isotopic samples per 10 million year bin.

paleo-oceans of deep time. In this paper we systematically investigate the isotopic composition of spreading ridge and plume-induced basaltic rocks preserved in ophiolites through time along suture zones formed during the assembly of Gondwana and Pangea, as well as samples from the present-day African mantle domain oceans, so to document the timing and extent of the mantle enrichment in the African domain.

### Clues from past oceans

The more recent full-plate paleogeographic reconstructions suggest that the transition from Rodinia to Pangea supercontinents occurred through the closure of Rodinia's external superocean, with the proto-Pacific Ocean formed during the break-up of Rodinia which later became the Pangean-time Panthalassa Superocean and now the Pacific Ocean<sup>13,16</sup>. Therefore, the mantle region that would eventually become the African mantle domain was initially the external oceanic area during 900–700 Ma. The mantle domain of the Rodinia external superocean (the Mirovoi Superocean; Supplementary Fig. 1) would have received little recycled material, at least since the time of Rodinia formation at 900 Ma. As Rodinia disaggregated and its constituent blocks drifted into the external ocean, the oceanic lithosphere in that space would get recycled, but fragments from some of those past oceans have been preserved in the Gondwana- and Pangea-forming sutures.

We compiled data from ophiolite belts of such lost oceans (and related minor seaways) as well as the Paleo-Tethys and Tethyan oceans, and some ophiolites in the Central Asian Orogenic Belt derived from the so-called Paleo-Asian Ocean (Supplementary Fig. 1). The present-day locations of the ophiolite samples are shown in Fig. 1b, and the

represented paleo-oceans and sample distributions are shown in Fig. 1c. These ophiolites can be linked back to now-closed paleo-oceanic basins using the geotectonic context of their surrounding terranes and global plate-tectonic reconstruction models<sup>16,17</sup>. This is demonstrated schematically in Supplementary Fig. 2.

In total, we compiled isotopic data from 88 such ophiolites. While there are 947 Nd isotopic analyses, Sr and Pb isotopic measurements are far less common (Supplementary Fig. 3). The data from ophiolites was used in combination with data from present-day oceanic lithosphere, including normal ocean floor basalts and plume-derived rocks. We focused on oceanic basalts because continental basalts are likely contaminated by continental crust during ascent and storage through the crust which makes any interpretation based on enriched isotopic signatures difficult. The Nd isotopic system not only has the largest number of analyses available in the dataset, but it is also resistant to alteration processes such as seawater alteration<sup>18</sup>. Therefore, we focus on the Nd isotopic system as a proxy for isotopic enrichment or depletion, because a low Nd isotopic ratio is the most definitive feature of the EM signature<sup>1–3,6</sup>. We divided the ophiolite dataset into two groups: plume-derived ophiolite samples and upper mantle-derived ophiolite samples, with the latter including both supra-subduction zone and mid-ocean ridge-related ophiolites (Supplementary Data 1). The ages of the ophiolites range from 900 to 70 Ma (Supplementary Data 1; Fig. 1). We group supra-subduction zone and ocean ridge basalts because Nd isotopes between basalts of these two environments are almost indistinguishable (Supplementary Fig. 4). The difference between the plume-related and upper mantle-derived samples is highlighted by their distinct incompatible trace element patterns (Supplementary Fig. 5).

A common way of expressing variations in Nd isotopes when studying mantle evolution is using  $\epsilon$ Nd as defined by DePaolo and Wasserburg<sup>19</sup>, which measures the deviation from the chondritic uniform reservoir (CHUR) reference line. The upper mantle, however, due to isotopic ingrowth, is constantly becoming more depleted relative to CHUR and, consequently, its  $\epsilon$ Nd is increasing over time<sup>20</sup>. Consequently, two samples with the same  $\epsilon$ Nd value but different ages might possess different degrees of depletion. For this reason, to compare the degree of depletion/enrichment in samples with distinct ages, we propose a new index  $\Delta_{DM}$  to measure the deviation of Nd isotope composition of a sample from the linear model-depleted mantle that has a present-day  $\epsilon$ Nd = 10, equivalent to a  $^{143}\text{Nd}/^{144}\text{Nd}$  ratio of 0.51314<sup>21</sup> (see Methods); when  $\Delta_{DM} < 0$ , the sample is more enriched than the depleted mantle, whereas when  $\Delta_{DM} > 0$  the sample is more depleted than the depleted mantle. Therefore, the lower the  $\Delta_{DM}$  value the more isotopically enriched a sample is in terms of Nd isotopes.

## Isotopic evolution of the African mantle domain through time

The upper mantle-derived and plume-derived rocks exhibit distinct evolution paths through time (Fig. 2). While the upper mantle-derived rocks present consistent scatter through time, their mean  $\Delta_{DM}$  values remain relatively constant throughout the post-900 Ma period. On the other hand, the plume-derived rocks display markedly decreased  $\Delta_{DM}$  values in late Phanerozoic, indicating a long period of increased isotopic enrichment. We modelled the evolution curve of the upper mantle and plume-derived rocks with a non-parametric Gaussian Process approach<sup>22</sup> (see Methods). The advantage of such a non-parametric approach is that it can account for the non-uniform distribution of data through time. The Gaussian Process approach models the way correlation between samples varies with distance, where correlation decreases with increasing distance<sup>22,23</sup>. In this case, distance refers to the time difference between samples. The regression results are shown in Fig. 2. The separation between plume- and upper mantle-derived rocks started from *ca.* 350 Ma, but becomes most striking after 200 Ma. Such results are consistent between different regression methods (Supplementary Fig. 6).

The regression curve for the upper mantle-derived rocks (Fig. 2a) is mostly flat, at  $\Delta_{DM} \sim -2.44$ , with some minor spikes. On the other hand, the plume-derived rocks display a roughly three-stage evolution in which the trend begins at a similar level to that of the upper mantle-derived rocks, i.e.,  $\Delta_{DM} = -3.5$ , but starts to decrease from  $\sim$ 350 Ma towards isotopic enrichment (more negative  $\Delta_{DM}$  values) with a minimum  $\Delta_{DM} = -6.87$  reached at 100–90 Ma, before it starts to increase again toward upper mantle value (Fig. 2b). The pattern of decrease in  $\Delta_{DM}$  values is also present if we only look at plume-derived ophiolites (Supplementary Fig. 7). This indicates that the enrichment trend observed is not an artefact of combining the ophiolite and present-day ocean datasets. Furthermore, the means of each 10 Ma bin for the plume-derived samples older than 300 Ma are significantly different at the 95% level from the means of the same sample size drawn from the present-day ocean plume Nd isotopic dataset (see Methods, Supplementary Fig. 8), ruling out the trend being due to sampling density bias. The increasing depletion trend in the data after the minimum  $\Delta_{DM}$  at 100–90 Ma may partly reflect increased volcanism in the northern hemisphere after 60 Ma, where rocks are generally more isotopically depleted, but even if only southern hemisphere rocks are considered a statistically significant depletion trend can still be observed (Supplementary Fig. 9).

We find further support for isotopic enrichment in the Palaeozoic by zooming in on samples showing extreme isotopic enrichment. Jackson et al.<sup>6</sup> suggested a threshold of 0.5126 for discriminating EM compositions. Here we opt to use the present-day  $^{143}\text{Nd}/^{144}\text{Nd}$  composition of the Chondritic Uniform Reservoir (CHUR)<sup>24</sup> as a threshold. By reconstructing the  $\Delta_{DM}$  CHUR evolution from 900 Ma, we observe that *ca.* 250 Ma Paleo-Tethyan plume-related rocks of the Tangjia-Sumdo ophiolite<sup>25</sup> were more enriched than CHUR. The regression results track the average African mantle domain plume source isotopic composition through time and show that a

fundamental change in the plume source had been underway since the beginning of the Late Palaeozoic, and the observation of extreme enrichment at the Palaeozoic-Mesozoic boundary is the result of a longer enrichment process.

## A geodynamic cause for the observed mantle isotopic anomalies

The EM signature in plume-derived rocks is commonly attributed to the recycling of crustal materials that are then incorporated into the sources of mantle plume<sup>1,2,9,10</sup>. Because of its high buoyancy, continental material introduced into the mantle is likely to be exhumed back to the crustal level, or relaminated to the base of the continental lithosphere<sup>26</sup>. The introduction of continental crustal material in the mantle can be attained by lower crust foundering, sedimentary subduction, subduction erosion, and wholesale continental crust subduction<sup>27</sup>. In a recent study, Jackson and MacDonald<sup>7</sup> suggested that the origin of the EM signature in the mantle was caused by the subduction of rifted passive margins starting at 650 Ma and, therefore, the input of continental crustal material into the mantle. This model explains the generally ancient isotopic signature commonly attributed to recycled materials<sup>7</sup>, as evidenced mostly by Pb isotopes<sup>1</sup> and mass-independent fractionated signatures in S isotopes<sup>28</sup>, although younger recycled crust materials of 650–200 Ma have also been proposed for some enriched plume sources based on Sr and Os isotopes<sup>29,30</sup>. However, the contribution of wholesale continental crust recycling in total crustal recycling is relatively minor compared to subduction erosion and sedimentary subduction<sup>27</sup>, all of which occur in convergent margins which were concentrated in the African domain over the last supercontinent cycle<sup>13,16</sup>. Therefore, crustal recycling that gave origin to the enriched mantle domains probably happened by a combination of different processes.

The geochemical evolution trend observed for the African mantle domain plume-derived rocks (from both ophiolites and present-day oceans) clearly demonstrates a post-1 Ga origin for the enriched isotopic signal. In addition, EM-signatures are much more widespread in the African mantle domain in comparison to the Pacific mantle domain, particularly prior to 20 Ma (Supplementary Fig. 10), when isotopically enriched volcanism such as that in the Pitcairn and Cook Islands started occurring<sup>31,32</sup>. Overall, our observations support the presence of an isotopic dichotomy on a hemispheric scale, with the African mantle domain inside the Circum-Pacific subduction girdle being more enriched than the Pacific mantle domain outside of the girdle<sup>12</sup>.

This interpretation is also supported by the observed *ca.* 350 Ma onset of the EM signal in the African mantle domain (Fig. 2). The estimates for the processing time of recycled material in the mantle vary, but estimates based on experiments<sup>33</sup>, and on the calculated slab sinking rates of 1.1 to 1.9 cm/yr<sup>34</sup> and plume upwelling times of up to 80–100 Myr<sup>35</sup>, are in the order of 200–300 Myr<sup>7</sup>. This lag time between crustal material input, entrainment in the plume source, and finally detection in the plume-derived magmas is consistent with the estimates presented here for the isotopic enrichment of the plume source in the African mantle domain: a *ca.* 300 Myr lag time between the *ca.* 650 Ma subduction of passive margin material associated with the assembly of Gondwana<sup>7</sup> and the *ca.* 350 Ma onset of the EM signal. This isotopic tipping point observed at the Late Palaeozoic for the plume source, marking a shift from a relatively steady PREMA-like signature to noticeable isotopic enrichment close to the Palaeozoic-Mesozoic boundary by 250 Ma (Fig. 2) is also close to the time estimate for the formation of an enriched kimberlite reservoir<sup>36</sup>. Continental crust material was likely also recycled back to the mantle before 650 Ma, but probably mostly into the Rodinia (present-day Pacific) mantle domain. Such an enrichment signal is thus not expected to be seen in the African domain, as shown by our observation (Fig. 2).

We use Fig. 3 to illustrate how the Rodinia-to-Pangea supercontinent cycle might have caused the observed mantle enrichment trend. After the breakup of Rodinia at *ca.* 700 Ma<sup>37</sup>, its constituent continental blocks drifted into the external oceanic domain (Fig. 3a, b). Some continental blocks later

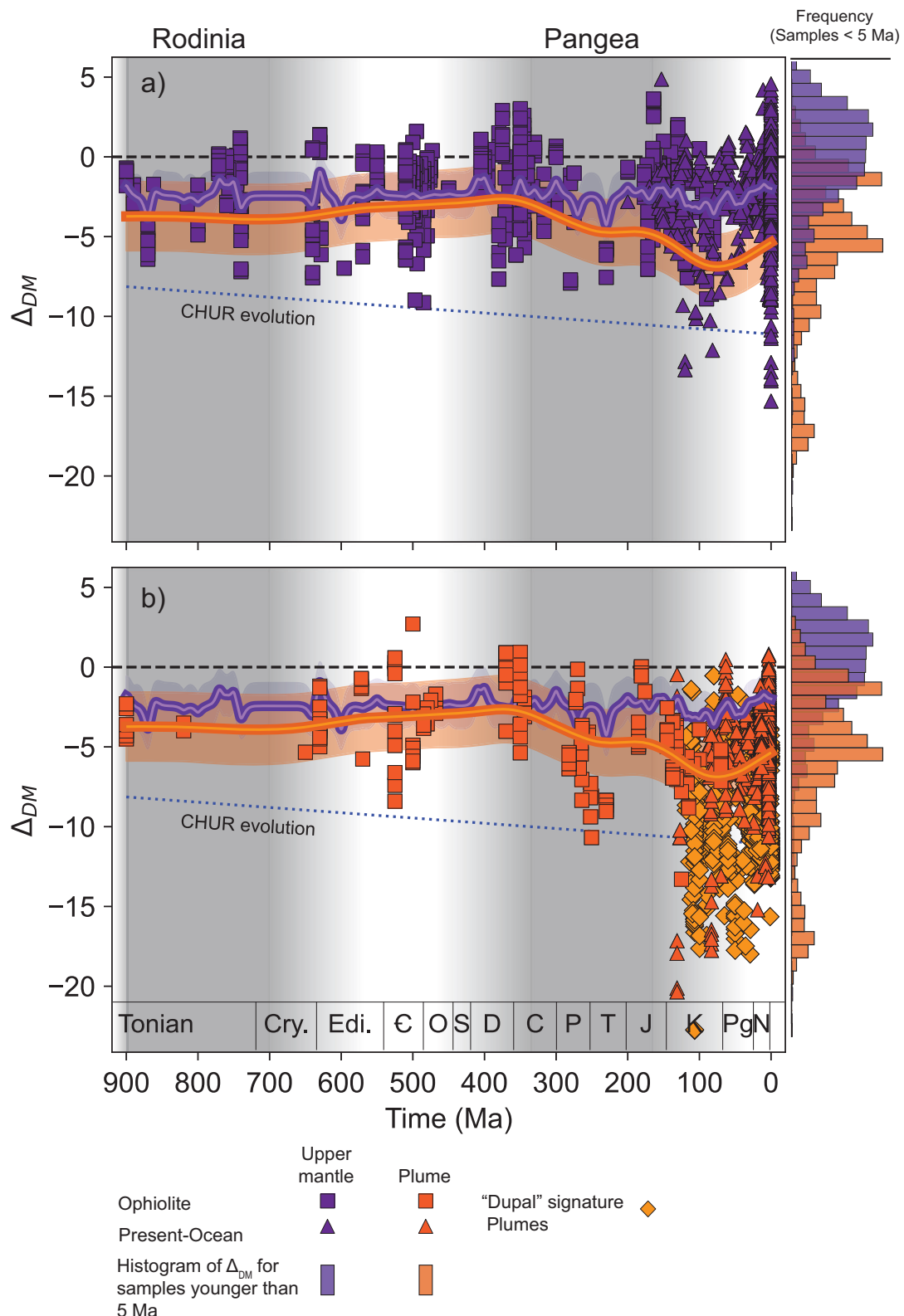


**Fig. 2 | Time evolution of the Nd isotopic composition.** Figure shows the deviation from the linear model-depleted mantle ( $\Delta_{DM}$ ) of samples from **a** upper mantle-derived and **b** plume-derived basalts. Both panels show the variation of  $\Delta_{DM}$  with time for ophiolite and present-day ocean samples of the African domain. The result of Gaussian process regression (see Methods) for each dataset is also shown. The results show a decoupling of the upper mantle trend from the plume trend after ca.

400 Ma. In the Late Cretaceous, the trend of plume-derived rocks reversed from an isotopic enrichment trend to a depletion one. The histogram on the right shows the  $\Delta_{DM}$  distribution for samples younger than 5 Ma. The Chondritic Uniform Reservoir (CHUR) evolution line is shown using present-day values of 0.51263 and 0.1960 for  $^{143}\text{Nd}/^{144}\text{Nd}$  and  $^{147}\text{Sm}/^{144}\text{Nd}$ , respectively<sup>24</sup>.

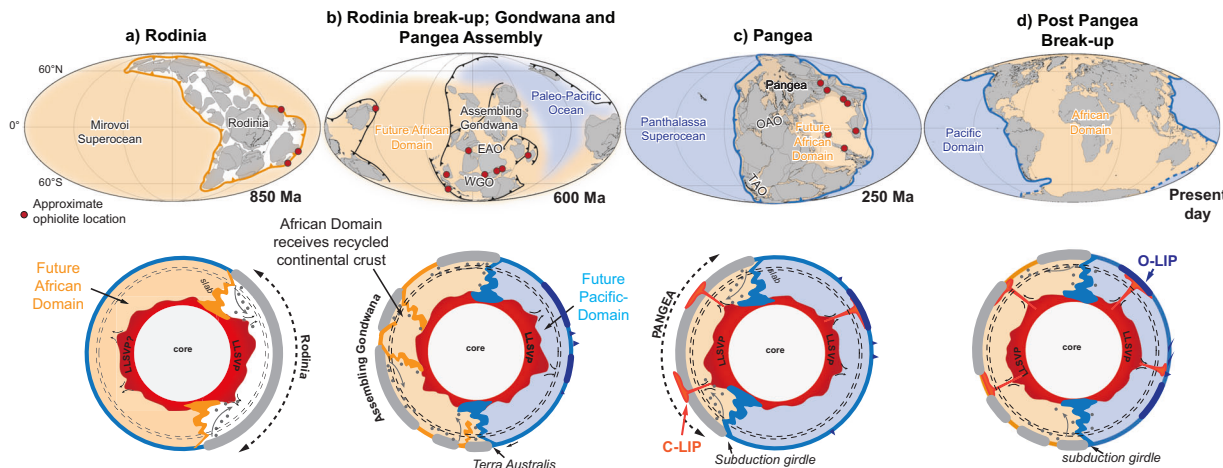


**Fig. 3 | Geodynamic synthesis.** Snapshots of the different geodynamic stages that led to isotopic enrichment in the African mantle domain. **a** During the existence of the supercontinent Rodinia, the region that would become the African domain (the Mirovoi Super Ocean surrounding Rodinia) received little recycled material. After Rodinia break-up, the reversal of subduction polarity led to the formation of Gondwana (**b**) and Pangea (**c**), preferentially recycling crustal material into the African domain by means of subduction toward the future African domain, collisional orogenies and, later, circum-supercontinent subduction<sup>12,13,16</sup>. After the break-up of Pangea (**d**), the new-born oceans (the Atlantic and Indian oceans) maintained

the recycled signature obtained during the previous stages as well as during the earlier stage of the break-up, but gradually became less enriched after 100–90 Ma when the expanding subduction girdle gradually parted the LLSVPs and plume generation zones<sup>50</sup>. The red circles represent the approximate locations of ophiolites within 50 Ma of the time depicted in each panel. EAO East African Orogen, WGO West Gondwana Orogen, OAO Ouachita-Alleghanian Orogen, TAO Terra Australis Orogen, C-LIP Continental Large Igneous Province, O-LIP Oceanic Large Igneous Province. The paleogeographical reconstructions in the figure are as in ref. 13.

collided to form Gondwana by ca. 540 Ma<sup>16</sup>. Coupled zircon U-Pb and Hf data indicate net continental loss during the amalgamation of Gondwana<sup>38</sup>, which suggests strong continental crustal recycling during this period, introducing low  $^{143}\text{Nd}/^{144}\text{Nd}$  material in the mantle. Moreover, Gondwana possessed large peripheral orogens (Terra Australis, Avalonian-Cadomian, North Indo-Australie)<sup>39</sup> that must have allowed for sustained input of crustal material into the African mantle domain through sedimentary subduction and subduction erosion, even before the formation of the circum-Pacific subduction girdle at Pangea times (Fig. 3c, d). Based on the almost continuous isotopic record provided by the ophiolites, we envisage a scenario where the transition from Rodinia to Gondwana during the Neoproterozoic, and accompanying change in subduction polarity along the margin of the growing Paleo-Pacific Ocean (Fig. 3a, b), that caused a switch in the recycled material accumulation locus<sup>12,13</sup> (Fig. 3). This switch coincided with the beginning of passive margin subduction at ca. 650 Ma, allowing wholesale continental subduction and a larger input of recycled material into the future African mantle domain (shown in beige colour in Fig. 3)<sup>7</sup>. Rodinia's external oceanic domain (future African mantle domain; Fig. 3a) therefore switched from receiving no recycled material to receiving the largest share of it, eventually yielding the enriched isotopic signature that characterises the African mantle domain. After the formation of Gondwana and eventually Pangea, the continued presence of the circum-African mantle domain subduction girdle (now the circum-Pacific subduction girdle) means that crustal materials would have continuously been recycled into the African mantle domain<sup>12</sup> (Fig. 3c, d), causing the steady enrichment through time past  $>600$  Ma. The origin of the enriched isotopic signal in the African mantle domain is thus a consequence of global geotectonic evolution since the Neoproterozoic, which concentrated subduction in the African mantle domain relative to the Pacific mantle domain, creating the prevalence of enriched isotopic signatures in the African Domain since late Palaeozoic.

We note that our analysis based on the reconstruction model of reference<sup>13</sup> remains valid for other recent global reconstruction models<sup>16,17</sup>. Although the shapes of oceanic basins might vary between reconstruction models, their relative positions in terms of continental break-up and amalgamation remain similar. For example, in all these models the Paleo-Pacific Ocean opened by the break-up of Rodinia between the present-day

eastern Australian and western North American margins (with or without South China and other continental blocks in-between), which eventually evolved into the Panthalassa superocean and now the Pacific Ocean. On the other hand, in all these models Pangaea assembled through the closure of the previous superocean, i.e., an extroversion assembly of Pangaea.

Our regression model also suggests that the plume sources in the African mantle domain are progressively becoming less enriched after the late Cretaceous time. We interpret this as a possible consequence of a reduction in recycled continental crustal material into the mantle of the African mantle domain as the subduction girdle grows larger and further away from the AMD plume source regions during Pangea's break-up (Fig. 3c, d). This would imply that large-scale geochemical anomalies in the mantle might be evolving features reflective of the planet's geodynamic evolution through time, instead of static features present since early Earth.

## Methods

### Data compilation

The samples presented in the isotopic dataset of ophiolites were compiled from 88 ophiolites with ages spanning from 900 to 70 Ma. The radiogenic ingrowth-correction ages were provided using the same references as the samples. Only tholeiitic alkaline and mafic samples with metamorphism not beyond amphibolite facies were considered in the compilation. The filtered dataset contains 947 samples, which were divided into four categories: MOR (mid-ocean ridge-like), SSZ (supra-subduction zone), OIB (ocean island basalt-like), and OPB (oceanic plateau-like). The categorisation was based on trace element signatures and geological context as documented in the literature. The Sm-Nd isotopic system was utilised because of its representativeness and resistance to alteration. This system is very resistant to alteration by seawater due to the low abundance of Sm and Nd in this fluid ( $8 \times 10^{-7}$  and  $4 \times 10^{-6}$  ppm, respectively<sup>18,40</sup>). Thus, even highly altered oceanic crust can still retain comparable  $^{143}\text{Nd}/^{144}\text{Nd}$  ratios to that of mid-ocean ridge basalts<sup>18</sup>.

The ophiolite data was used together with data from samples from present-day oceans to build a full evolutionary picture. Data from mid-ocean ridges in the African domain (the Atlantic, Indian and Arctic oceans) was taken from the compilation of Stracke et al.<sup>41</sup>. We also used data from old oceanic crust compiled from PetDB (<https://earthchem.org/>). Where

age data was not readily available for the ocean floor samples in PetDB, we utilised a 6-arc minute resolution age grid of the present-day ocean floor based on the Seton et al.<sup>14</sup> model of ocean floor ages to estimate the age for the sample.

Current oceanic plume data used were collected from the compilations of Homrighausen et al.<sup>42</sup> and Olierook et al.<sup>43</sup> for the Tristan-Walvis and Kerguelen plumes, respectively, and from the compilation of Stracke et al.<sup>41</sup> for Réunion, Iceland, Faroe Islands, Jan Mayen, Madeira, Ascension, Amsterdam and St. Paul, Canary Islands, Cape Verde and Azores. We also compiled data from the Crozet, Afanasy-Nikitin, Discovery, Meteor-Shona and Trindade tracks (see relevant references in Supplementary Data 1).

### Δ<sub>DM</sub> calculation

Delta DM was calculated as the deviation from a linear model depleted mantle<sup>21</sup> in the same way, as ε<sub>Nd</sub> is calculated as a deviation from the CHUR evolution line. Depleted mantle values were back-calculated using present-day <sup>147</sup>Sm/<sup>144</sup>Nd and <sup>143</sup>Nd/<sup>144</sup>Nd values of 0.222<sup>44</sup> and 0.51314<sup>21</sup>, respectively. For samples with initial ε<sub>Nd</sub> reported but without the Nd isotopic ratio, the initial ratio was estimated from the ε<sub>Nd</sub> value. The equation for calculating Δ<sub>DM</sub> is similar to that of ε<sub>Nd</sub>:

$$\Delta_{DM} = \left( \frac{(^{143}Nd / ^{144}Nd)_{Sample,t}}{(^{143}Nd / ^{144}Nd)_{DM,t}} - 1 \right) * 10^4$$

### Statistical methods

Given the non-uniform sample distribution through time, we adopted a non-parametric approach for regression of Δ<sub>DM</sub> values. We utilised Gaussian Process regression<sup>22</sup> through the scikit-learn library (version 1.2.2)<sup>45</sup> for Python. Δ<sub>DM</sub> values were pooled into bins of 10 million years, and the mean value of each bin was used as the input value for the regression. Plume-related rocks (OIB and OPB) and upper mantle-related (MOR and SSZ) were treated separately. For both plume and upper mantle rocks, the Kernel was set as a sum of constant kernel (modifier of the mean of the Gaussian process), Matérn kernel (with ν = 1.5) and white noise kernel. The hyperparameters for each dataset were optimised by attempting to maximise the log marginal likelihood of the model using the built-in scikit-learn algorithm. The optimised length scales for the Matérn kernels were 75.3 and 5.64 for the plume and upper mantle-related rocks, respectively. The other regression methods used for comparison with the Gaussian Process were the generalised additive model (GAM) smoothing<sup>23,46</sup>, with adaptative and thin-plate smoothing and LOWESS<sup>47</sup>. The GAMs were fitted using the mgcv<sup>48</sup> package for R. In the GAM approach, the means of each 10 Ma bin were weighted by the number of samples used to calculate the mean. The adaptative GAM smooth for the plume-related rocks had 3.88 effective degrees of freedom (edf) with a p-value of 1.34\*10<sup>-6</sup> and 72% of deviance explained, whereas for the upper mantle-related rocks the edf was 2.612 with a non-significant p-value of 0.0528 and 16.8% of deviance explained. The thin-plate GAM smooth had a higher edf of 5.779 and a p-value of 2.06\*10<sup>-5</sup> and 71.4% of deviance explained for the plume-related rocks. Thin-plate regression for the upper mantle-related rocks has an edf of 2.955 with a non-significant p-value of 0.366 and 12% deviance explained. The LOWESS was fit with the statsmodels package for Python (v. 0.14.0)<sup>49</sup>.

To account for sampling bias, we compared the means of each of the 10 Ma bins of the plume dataset to the means of one thousand re-sampling of the same sample size drawn from the Nd isotopic dataset of present-day plume-derived rocks in order to test the statistical significance of the limited sample sizes per age bin. For example, if 15 analyses were used to determine the mean at a given age bin, the means of 1000 sets of 15 analyses drawn from the present-day dataset were used to determine the confidence intervals at the 1σ (68%) and 2σ (95%) levels. Although for some samples older than 300 Ma, the mean is not distinguishable from the present-day distribution at the 95% confidence level, the mean Δ<sub>DM</sub> value for rocks older

than 300 Ma is significantly different at the 95% confidence level from the present-day distribution, while for rocks younger than 300 Ma the means cannot be statistically distinguished (Supplementary Fig. 8).

### Data availability

Supplementary Data 1 contains all the supporting data for this article and can be accessed at: [https://figshare.com/articles/dataset/SupplementaryTable1\\_xlsx/26242157](https://figshare.com/articles/dataset/SupplementaryTable1_xlsx/26242157).

Received: 28 February 2024; Accepted: 14 August 2024;

Published online: 28 August 2024

### References

1. Hofmann, A. W. Mantle geochemistry: the message from oceanic volcanism. *Nature* **385**, 219–229 (1997).
2. White, W. M. Isotopes, DUPAL, LLSVPs, and Anekantavada. *Chem. Geol.* **419**, 10–28 (2015).
3. Zindler, A. & Hart, S. Chemical geodynamics. *Annu. Rev. Earth Planet. Sci.* **14**, 493–571 (1986).
4. Dupré, B. & Allègre, C. J. Pb-Sr isotope variation in Indian Ocean basalts and mixing phenomena. *Nature* **303**, 142–146 (1983).
5. Hart, S. R. A large-scale isotope anomaly in the Southern Hemisphere mantle. *Nature* **309**, 753–757 (1984).
6. Jackson, M., Becker, T. & Steinberger, B. Spatial characteristics of recycled and primordial reservoirs in the deep mantle. *Geochem. Geophys. Geosyst.* **22**, e2020GC009525 (2021).
7. Jackson, M. G. & Macdonald, F. Hemispheric geochemical dichotomy of the mantle is a legacy of austral supercontinent assembly and onset of deep continental crust subduction. *AGU Adv.* **3**, e2022AV000664 (2022).
8. Konter, J. G. et al. One hundred million years of mantle geochemical history suggest the retiring of mantle plumes is premature. *Earth Planet. Sci. Lett.* **275**, 285–295 (2008).
9. Hofmann, A. W. & White, W. M. Mantle plumes from ancient oceanic crust. *Earth Planet. Sci. Lett.* **57**, 421–436 (1982).
10. Willbold, M. & Stracke, A. Formation of enriched mantle components by recycling of upper and lower continental crust. *Chem. Geol.* **276**, 188–197 (2010).
11. Staudigel, H. et al. The longevity of the South Pacific isotopic and thermal anomaly. *Earth Planet. Sci. Lett.* **102**, 24–44 (1991).
12. Doucet, L. S. et al. Distinct formation history for deep-mantle domains reflected in geochemical differences. *Nat. Geosci.* **13**, 511–515 (2020).
13. Li, Z. X. et al. Decoding Earth's rhythms: modulation of supercontinent cycles by longer superocean episodes. *Precambrian Res.* **323**, 1–5 (2019).
14. Seton, M. et al. A global data set of present-day oceanic crustal age and seafloor spreading parameters. *Geochem. Geophys. Geosyst.* **21**. <https://doi.org/10.1029/2020gc009214> (2020).
15. Dilek, Y. Ophiolite concept and its evolution. *Special Papers-Geological Society of America*. 1–16 (Geological Society of America, 2003).
16. Li, Z.-X., Liu, Y. & Ernst, R. A dynamic 2000–540 Ma Earth history: from cratonic amalgamation to the age of supercontinent cycle. *Earth Sci. Rev.* **238**, 104336 (2023).
17. Merdith, A. S. et al. Extending full-plate tectonic models into deep time: linking the neoproterozoic and the phanerozoic. *Earth Sci. Rev.* **214**, 103477 (2021).
18. Staudigel, H., Davies, G., Hart, S. R., Marchant, K. & Smith, B. M. Large scale isotopic Sr, Nd and O isotopic anatomy of altered oceanic crust: DSDP/ODP sites 417/418. *Earth Planet. Sci. Lett.* **130**, 169–185 (1995).
19. DePaolo, D. J. & Wasserburg, G. Nd isotopic variations and petrogenetic models. *Geophys. Res. Lett.* **3**, 249–252 (1976).

20. DePaolo, D. J. Crustal growth and mantle evolution: inferences from models of element transport and Nd and Sr isotopes. *Geochim. Cosmochim. Acta* **44**, 1185–1196 (1980).

21. Goldstein, S. L., O’Nions, R. K. & Hamilton, P. J. A Sm–Nd isotopic study of atmospheric dusts and particulates from major river systems. *Earth Planet. Sci. Lett.* **70**, 221–236 (1984).

22. Rasmussen, C. E. & Williams, C. K. *Gaussian Processes for Machine Learning*. Vol. 1 (Springer, 2006).

23. Simpson, G. L. Modelling palaeoecological time series using generalised additive models. *Front. Ecol. Evol.* **6**, 149 (2018).

24. Bouvier, A., Vervoort, J. D. & Patchett, P. J. The Lu–Hf and Sm–Nd isotopic composition of CHUR: constraints from unequilibrated chondrites and implications for the bulk composition of terrestrial planets. *Earth Planet. Sci. Lett.* **273**, 48–57 (2008).

25. Wang, B. et al. A greenstone belt in southeast Tibet: an accreted middle–late Permian oceanic plateau. *Geosci. Front.* **14**, 101534 (2023).

26. Hacker, B. R., Kelemen, P. B. & Behn, M. D. Differentiation of the continental crust by relamination. *Earth Planet. Sci. Lett.* **307**, 501–516 (2011).

27. Stern, R. J. & Scholl, D. W. Yin and yang of continental crust creation and destruction by plate tectonic processes. *Int. Geol. Rev.* **52**, 1–31 (2010).

28. Cabral, R. A. et al. Anomalous sulphur isotopes in plume lavas reveal deep mantle storage of Archaean crust. *Nature* **496**, 490–493 (2013).

29. Sobolev, A. V., Hofmann, A. W., Jochum, K. P., Kuzmin, D. V. & Stoll, B. A young source for the Hawaiian plume. *Nature* **476**, 434–437 (2011).

30. Wang, X.-C. et al. Identification of an ancient mantle reservoir and young recycled materials in the source region of a young mantle plume: Implications for potential linkages between plume and plate tectonics. *Earth Planet. Sci. Lett.* **377**, 248–259 (2013).

31. Guillou, H., Garcia, M. O. & Turpin, L. Unspiked K–Ar dating of young volcanic rocks from Loihi and Pitcairn hot spot seamounts. *J. Volcanol. Geotherm. Res.* **78**, 239–249 (1997).

32. Rose, J. & Koppers, A. A. P. Simplifying age progressions within the Cook–Austral islands using ARGUS–VI high-resolution 40Ar/39Ar incremental heating ages. *Geochim. Geophys. Geosyst.* **20**, 4756–4778 (2019).

33. Zhong, J.-Q. & Zhang, J. Thermal convection with a freely moving top boundary. *Phys. Fluids* **17**, 115105 (2005).

34. Domeier, M., Doubrovine, P. V., Torsvik, T. H., Spakman, W. & Bull, A. L. Global correlation of lower mantle structure and past subduction. *Geophys. Res. Lett.* **43**, 4945–4953 (2016).

35. Steinberger, B., Nelson, P., Grand, S. & Wang, W. Yellowstone plume conduit tilt caused by large-scale mantle flow. *Geochim. Geophys. Geosyst.* **20**, 5896–5912 (2019).

36. Giuliani, A., Jackson, M. G., Fitzpayne, A. & Dalton, H. Remnants of early Earth differentiation in the deepest mantle-derived lavas. *Proc. Natl Acad. Sci. USA* **118**, e2015211118 (2021).

37. Li, Z.-X. et al. Assembly, configuration, and break-up history of Rodinia: a synthesis. *Precambrian Res.* **160**, 179–210 (2008).

38. Roberts, N. M. Increased loss of continental crust during supercontinent amalgamation. *Gondwana Res.* **21**, 994–1000 (2012).

39. Cawood, P. A., Martin, E. L., Murphy, J. B. & Pisarevsky, S. A. Gondwana’s interlinked peripheral orogens. *Earth Planet. Sci. Lett.* **568**, 117057 (2021).

40. McCulloch, M. T., Gregory, R. T., Wasserburg, G. & Taylor, H. P. Jr Sm–Nd, Rb–Sr, and  $^{18}\text{O}/^{16}\text{O}$  isotopic systematics in an oceanic crustal section: evidence from the Samail Ophiolite. *J. Geophys. Res. Solid Earth* **86**, 2721–2735 (1981).

41. Stracke, A., Willig, M., Genske, F., Béguelin, P. & Todd, E. Chemical geodynamics insights from a machine learning approach. *Geochim. Geophys. Geosyst.* **23**, e2022GC010606 (2022).

42. Homrighausen, S. et al. Evidence for compositionally distinct upper mantle plumelets since the early history of the Tristan–Gough hotspot. *Nat. Commun.* **14**, 3908 (2023).

43. Olieroock, H. K., Merle, R. E. & Jourdan, F. Toward a Greater Kerguelen large igneous province: evolving mantle source contributions in and around the Indian Ocean. *Lithos* **282**, 163–172 (2017).

44. Michard, A., Gurriet, P., Soudant, M. & Albarede, F. Nd isotopes in French Phanerozoic shales: external vs. internal aspects of crustal evolution. *Geochim. Cosmochim. Acta* **49**, 601–610 (1985).

45. Pedregosa, F. et al. Scikit-learn: machine learning in Python. *J. Mach. Learn. Res.* **12**, 2825–2830 (2011).

46. Wood, S. N. *Generalized Additive Models: an Introduction with R*. (CRC press, 2017).

47. Cleveland, W. S. Robust locally weighted regression and smoothing scatterplots. *J. Am. Stat. Assoc.* **74**, 829–836 (1979).

48. Wood, S. & Wood, M. S. Package ‘mgcv’. *R. Package Version 1*, 729 (2015).

49. Seabold, S. & Perktold, J. Statsmodels: Econometric and Statistical Modeling with Python. In *Proceedings of the 9th Python in Science Conference* 92–96 (2010).

50. Burke, K., Steinberger, B., Torsvik, T. H. & Smethurst, M. A. Plume generation zones at the margins of large low shear velocity provinces on the core–mantle boundary. *Earth Planet. Sci. Lett.* **265**, 49–60 (2008).

## Acknowledgements

This study was supported by the Australian Research Council Laureate Fellow grant (FL150100133) and the National Natural Science Foundation of China PGP RFIS-III grant (42350710792) awarded to ZXL. PABS would like to acknowledge Curtin University for PhD scholarship no. RES55354. We thank Jiten Pattnaik and two anonymous reviewers for their comments and suggestions.

## Author contributions

P.A.B.S.: writing—original draft, visualisation, conceptualisation, methodology, investigation, data curation. Z.X.L.: writing—review and editing, conceptualisation, visualisation, supervision, funding acquisition. L.S.D.: writing—review and editing, conceptualisation, visualisation, supervision.

## Competing interests

The authors declare no competing interests.

## Additional information

**Supplementary information** The online version contains supplementary material available at <https://doi.org/10.1038/s43247-024-01627-w>.

**Correspondence** and requests for materials should be addressed to Piero A. B. de Sampaio or Zheng-Xiang Li.

**Peer review information** *Communications Earth & Environment* thanks Nicolas Flament, Jiten Pattnaik and the other, anonymous, reviewer(s) for their contribution to the peer review of this work. Primary handling editor: Carolina Ortiz Guerrero. A peer review file is available.

**Reprints and permissions information** is available at <http://www.nature.com/reprints>

**Publisher’s note** Springer Nature remains neutral with regard to jurisdictional claims in published maps and institutional affiliations.

**Open Access** This article is licensed under a Creative Commons Attribution-NonCommercial-NoDerivatives 4.0 International License, which permits any non-commercial use, sharing, distribution and reproduction in any medium or format, as long as you give appropriate credit to the original author(s) and the source, provide a link to the Creative Commons licence, and indicate if you modified the licensed material. You do not have permission under this licence to share adapted material derived from this article or parts of it. The images or other third party material in this article are included in the article's Creative Commons licence, unless indicated otherwise in a credit line to the material. If material is not included in the article's Creative Commons licence and your intended use is not permitted by statutory regulation or exceeds the permitted use, you will need to obtain permission directly from the copyright holder. To view a copy of this licence, visit <http://creativecommons.org/licenses/by-nc-nd/4.0/>.

© The Author(s) 2024